Journal of Analytical and Applied Pyrolysis 151 (2020) 104918

Contents lists available at ScienceDirect

Journal of Analytical and Applied Pyrolysis

journal homepage: www.elsevier.com/locate/jaap

Analyses of the thermal characteristics and gaseous products of guanidine nitrate/basic copper nitrate mixtures using calorimetry with high resolution mass spectrometry

Yu-ichiro Izato [a,b,*], Kento Shiota [b], Kenta Satoh [c], Takashi Satoh [d], Yukinori Yahata [d], Atsumi Miyake [b]

[a] Graduate School of Environment and Information Sciences, Yokohama National University, 79-7 Tokiwadai, Hodogaya-ku, Yokohama, Kanagawa 240-8501, Japan
[b] Institute of Advanced Sciences, Yokohama National University, 79-5 Tokiwadai, Hodogaya-ku, Yokohama, Kanagawa 240-8501, Japan
[c] Application Group, NETZSCH Japan K.K., 3-9-13, Moriya-cho, Kanagawa-ku, Yokohama, Kanagawa 221-0022, Japan
[d] MS Research and Development Department, MS Business Unit, JEOL Ltd., 3-1-2 Musashino, Akishima, Tokyo 196-8558, Japan

ARTICLE INFO

Keywords:
Guanidine nitrate
Basic copper nitrate
Evolved gas analysis
High resolution spectrometry

ABSTRACT

This work assessed the pyrolysis of a well-established gas generating agent consisting of a mixture of guanidine nitrate (GN) with basic copper nitrate (BCN), using thermogravimetry-differential scanning calorimetry in conjunction with high resolution mass spectrometry (TG/DSC/HRMS). This instrumentation simultaneously determined mass changes and heat flow, and also permitted evaluation of evolved gases on an accurate mass basis. Fragmentation ratio correction was used to analyze the MS data acquired via electron ionization. GN/BCN mixtures were found to undergo pyrolysis to evolve H_2O, N_2, $NO^{\bullet}$, CO_2 and N_2O. Using HRMS, species having similar masses, such as CO_2 and N_2O, CO and N_2, and NH_3 and $OH^{\bullet}$, were successfully distinguished. The thermal analysis data and the gas evolution results allowed a pyrolysis mechanism to be proposed. In this mechanism, a copper(II) complex obtained from the BCN catalytically decomposes NH_3 generated from the GN to produce N_2 and H_2O. The pyrolysis of a mixture of GN and BCN thus provides a synergistic effect that increases the heat and gas output.

1. Introduction

Gas generation compounds such as those used in automobile airbag systems must be capable of rapidly evolving large quantities of gaseous products via exothermic reactions. These systems are thus based on energetic materials that store energy in their chemical structures and can be employed to generate heat and pressure when initiated. The substances in such devices must also be chemically and mechanically stable, demonstrate adequate burning rates under various pressures, and ideally produce large amounts of nontoxic gases with minimal solid residue. Mixtures in which guanidine nitrate (GN) acts as a fuel and basic copper nitrate (BCN; $Cu_2(NO_3)(OH)_3$) acts as an oxidizer (GN/BCN) are currently well-established as gas generating agents and have been widely applied in automobile airbag systems [1]. To date, GN/BCN mixtures have satisfied the requirements for gas generation in such systems. However, increasingly strict regulations and the requirements to achieve smaller and lighter airbag inflators require improvements in the performance of such mixtures. Specifically, the flame temperature, solid residue generation and toxicity of the evolved gases must all be improved. There have been significant efforts devoted to mitigating the disadvantages of GN/BCN systems or to enhancing the performance of these mixtures, as well as to developing novel gas generators as alternatives.

A detailed understanding of the reason for the improved performance as well as the potential disadvantages of such novel generating systems is helpful for the effective development of next generation gas evolution agents. To this end, the reaction mechanisms for a wide range of highly energetic materials have been studied based on various analytical techniques by many researchers [2–7]. Thermal analysis combined with evolved gas analysis (TA/EGA) has been frequently used for this purpose. In particular, TA/EGA based on thermogravimetry (TG)/differential scanning calorimetry (DSC) or /differential thermal

* Corresponding author at: Graduate School of Environment and Information Sciences, Yokohama National University, 79-7 Tokiwadai, Hodogaya-ku, Yokohama, Kanagawa 240-8501, Japan.
E-mail address: izato-yuichiro-tk@ynu.ac.jp (Y.-i. Izato).

https://doi.org/10.1016/j.jaap.2020.104918
Received 22 June 2020; Received in revised form 1 September 2020; Accepted 1 September 2020
Available online 5 September 2020

analysis (DTA) together with mass spectrometry (MS) and infrared (IR) spectroscopy are powerful tools for investigating the reaction mechanisms for energetic materials. These techniques can assess gas evolution characteristics while determining the thermal profile of the material, and can thus provide significant insights into reaction mechanisms. For these reasons, thermal and evolved gas analyses have been employed in studies of GN and GN/BCN mixtures [8–13] and to a wide range of other energetic compounds [14–18].

Even so, present-day TG/MS and /IR techniques have several drawbacks when applied to the assessment of energetic materials. These substances typically undergo pyrolysis to generate NH_3, H_2O, CO, N_2, $NO^{\bullet}$, CO_2, N_2O, $NO_2^{\bullet}$ and HNO_3, some of which are difficult to distinguish based on low-resolution MS data. As examples, the members of the CO_2 and N_2O, CO and N_2, and NH_3 and $OH^{\bullet}$ (representing a H_2O fragment) pairs have similar *m/z* values to one another. IR spectroscopy can distinguish between CO_2 and N_2O but cannot detect species that do not absorb in the IR range. The inability of IR analysis to detect N_2 can be especially problematic when studying the reaction mechanisms for energetic materials, because N_2 is nontoxic and thus the most desirable gaseous product from combustion and pyrolysis processes. These drawbacks have limited our understanding of the pyrolysis of energetic compounds, including GN/BCN mixtures, many of which generate gases that are difficult to conclusively identify with MS and IR techniques.

The aim of the present study was to investigate the gases evolved from GN/BCN mixtures, using TG and DSC in conjunction with high-resolution MS (HRMS). The latter technique offers the advantages of rapid scanning and acquisition of the full mass spectra of the fragment ions of compounds on an accurate mass basis. HRMS has the potential to address the disadvantages associated with standard MS and IR methods and so to provide additional insights into the reaction mechanisms for GN/BCN mixtures. The present study used this technique and also applied fragmentation ratio correction to the MS data to provide a better understanding of the gas evolution behavior of GN/BCN mixtures.

2. Experimental methods

2.1. Materials

TA/EGA assessments were conducted with pure BCN and GN as well as GN/BCN mixtures. Powdered GN (97 % purity) and BCN (98 % purity) were purchased from Fujifilm Wako Pure Chemical Industries, Ltd. and Nihon Kagaku Sangyo Co., Ltd., respectively, and used as received. GN/BCN mixtures were prepared manually in glass ampoules at a molar ratio of 9:4, based on the stoichiometry required for complete combustion by the reaction $9\,GN + 4\,BCN \rightarrow 9\,CO_2 + 20\,N_2 + 33\,H_2O + 9\,Cu$ [9].

2.2. TG/DTA/MS

TG/DTA/MS analyses were conducted to assess the pyrolysis of BCN. BCN contains Cu, H, N and O but not C, and so HRMS was not a helpful analytical tool in this case. The TG-DTA-MS apparatus consisted of an STA 2500 Regulus thermogravimetric analyzer (Netsczh) and a JMS-Q1050GC instrument (JEOL) equipped with an in-line EGA accessory (Netsczh). An approximately 3.0 mg quantity of BCN was placed in an aluminum pan (ϕ 5.2 mm × 5.1 mm) and heated from 50 to 400 °C at 10 °C min^{-1} under a continuous 50 mL min^{-1} He purge. An empty Al pan was used as a reference. Prior to heating, the TG-DTA instrument was evacuated for 5 min and then filled with He to a pressure of 1 atm. The gaseous decomposition products were analyzed using the MS instrument connected to the TG-DTA apparatus by a heated quartz capillary (I.D. 0.5 mm ×5 m, 300 °C), operating in electron ionization mode with an acceleration voltage of 70 eV and scanning over the *m/z* range from 10 to 100.

2.3. TG/DSC/HRMS

TG/DSC/HRMS analyses were conducted in conjunction with the pyrolysis of both pure GN and GN/BCN mixtures. The TG-DSC-high resolution time of flight mass spectrometer (HRTOFMS) apparatus consisted of an STA 449 F1 Jupiter thermogravimetric analyzer (Netsczh) and a JMS-MT3010HRGA INFITOF instrument (JEOL) equipped with an in-line EGA accessory (Netsczh). The latter featured a multi-turn technology that provided a variable length ion flight path of up to 200 m in a very compact analyzer (200 mm × 200 mm). The experimental procedure was similar to that employed during the TG-DTA-MS experiments, as described in Section 2.2. In each trial, an approximately 5.0 mg (GN) or 1.0 mg (GN/BCN) sample was placed in an aluminum pan (ϕ 6.7 mm × 2.7 mm) and heated from 30 to 350 °C at 10 or 5 °C min^{-1}, respectively, under a continuous 100 mL min^{-1} helium purge. A smaller sample size was used for the GN/BCN to avoid self-heating, while a slower heating rate was applied so as to differentiate the two exothermic peaks generated by this mixture. These peaks are known to overlap at a heating rate of 10 °C min^{-1} [9,11]. Prior to heating, the TG-DSC instrument was evacuated for 5 min and then filled with He to a pressure of 1 atm. An empty Al pan was used as a reference. The gaseous decomposition products were analyzed using the HRTOFMS instrument connected to the TG-DSC apparatus by a heated quartz capillary held at 300 °C. This unit was operated in electron ionization mode at 70 eV, with scanning over the *m/z* range from 10 to 100. The resolution of this instrument was 10,000 full width at half maximum, which was sufficient to identify the evolved gases in this study.

3. Results and discussion

3.1. TG/DTA/MS analysis of gas evolution with BCN

The TG/DTA/MS data demonstrated that the BCN exhibited an endothermic reaction accompanied by a mass loss and gas evolution beginning at approximately 200 °C (Fig. 1). MS peaks at *m/z* values of 18 (H_2O^+), 30 (NO^+), 32 (O_2^+), 44 (N_2O^+), 46 (NO_2^+) and 63 (HNO_3^+) were observed. These results are in agreement with prior reports concerning the MS analysis of BCN [9,10]. These data established that the primary evolved gases were H_2O, $NO^{\bullet}$, O_2, $NO_2^{\bullet}$, and HNO_3.

The MS profiles obtained from the BCN were examined using the fragmentation ratio correction method. When employing electron ionization, the gaseous products are typically fragmented into smaller species, and the fragmentation ratios for NH_3, H_2O, $NO^{\bullet}$ and $NO_2^{\bullet}$ at an acceleration voltage of 70 eV are provided in a NIST database [19] while that for HNO_3 can be found in the literature [20]. The supporting information provides an example on how the ratio values were obtained from the fragmentation correction method. The associated calculations are presented below as Eqs. 1 through 5.

$$I^{\text{total}}_{HNO_3} \cong I^{63}_{HNO_3^+}\left(HNO_3^+\right) + I^{46}_{NO_2^+}\left(HNO_3^+\right) + I^{30}_{NO^+}\left(HNO_3^+\right) = I^{63}_{HNO_3^+} + \frac{100}{2.04} I^{63}_{HNO_3^+} + \frac{85.7}{2.04} I^{63}_{HNO_3^+} \quad (1)$$

$$I^{\text{total}}_{NO_2\cdot} \cong I^{46}_{NO_2^+}\left(NO_2^+\right) + I^{30}_{NO^+}\left(NO_2^+\right) - I^{46}_{NO_2^+}\left(HNO_3^+\right) = I^{46}_{NO_2^+} + \frac{3703}{9999}\left(I^{46}_{NO_2^+} - \frac{100}{2.04} I^{63}_{HNO_3^+}\right) - \frac{100}{2.04} I^{63}_{HNO_3^+} \quad (2)$$

$$I^{\text{total}}_{NO\cdot} \cong I^{30}_{NO^+} - I^{30}_{NO^+}\left(NO_2^+\right) - I^{30}_{NO^+}\left(HNO_3^+\right) = I^{30}_{NO^+} - \frac{9999}{3703}\left(I^{46}_{NO_2^+} - \frac{100}{2.04} I^{63}_{HNO_3^+}\right) - \frac{85.7}{2.04} I^{63}_{HNO_3^+} \quad (3)$$

$$I^{\text{total}}_{O_2} \cong I^{32}_{O_2^+} + I^{16}_{O^+\left(O_2^+\right)} = I^{32}_{O_2^+} + \frac{2180}{9999} I^{32}_{O_2^+} \quad (4)$$

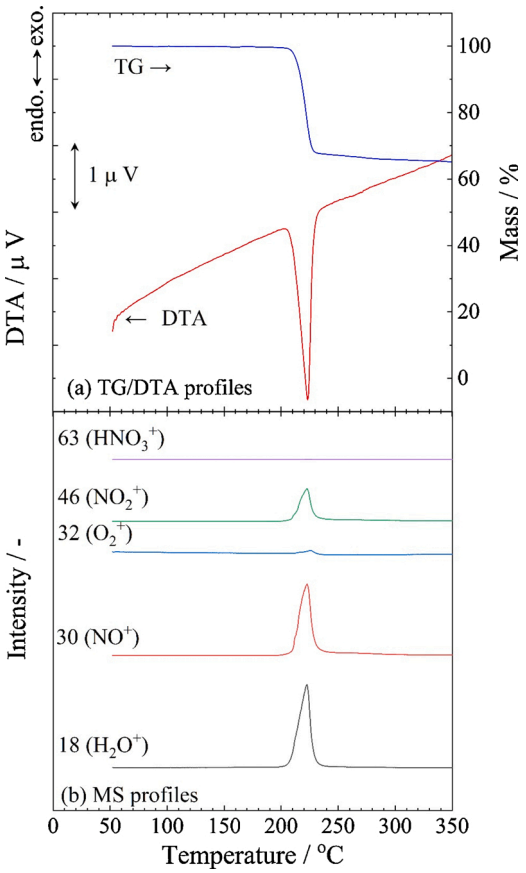

Fig. 1. (a) TG/DTA data and (b) MS profiles acquired from BCN at a heating rate of 10 °C min^{-1}.

$$I^{\text{total}}_{H_2O} \cong I^{18}_{H_2O^+} + I^{17}_{OH^+(H_2O^+)} = I^{18}_{H_2O^+} + \frac{2122}{9999} I^{18}_{H_2O^+} \quad (5)$$

Here, $I^{n}_{i\,(f)}$ is the relative intensity of the MS peak for ionized gas i or ion fragment i having $m/z = n$ and related to species f. Using these calculations, the relative intensity plots in Fig. 2 were obtained.

Fig. 2 summarizes the evolution of various gases from BCN at a heating rate of 10 °C min^{-1} and demonstrates that the primary pyrolysis products were H_2O, O_2, $NO_2^{\bullet}$ and HNO_3. Note that, although an intense peak is observed at $m/z = 30$ (corresponding to NO^+) in Fig. 1, the $NO^{\bullet}$ peak in Fig. 2 is minimal. This is because the majority of the NO^+ observed in the MS data is believed to have been derived from HNO_3 and $NO_2^{\bullet}$. Thus, this fragmentation ratio method prevented the overestimation of $NO^{\bullet}$ generation and is a helpful means of identifying evolved gas species from fragmentation patterns in electron ionization data.

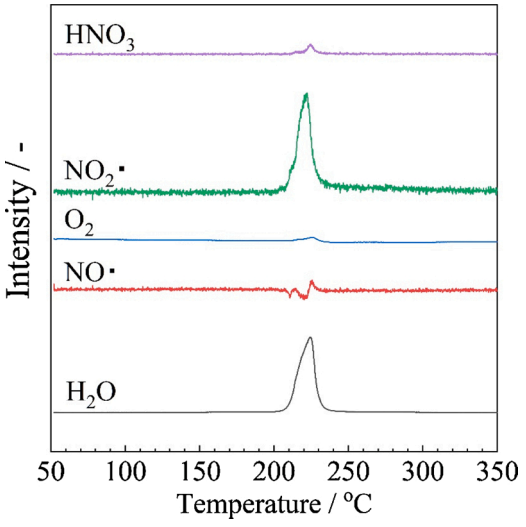

Fig. 2. The gas-evolution behavior of BCN at 10 °C min^{-1} based on MS data.

Based on the above results, it is possible to examine potential reaction mechanisms. BCN has the formula $Cu_2(NO_3)(OH)_3$ and thus is a double salt comprising a copper(II) cation with nitrate and hydroxide anions. Thus, BCN can be assumed to initially decompose simply to copper(II) nitrate ($Cu(NO_3)_2$) and copper(II) hydroxide ($Cu(OH)_2$). These two salts are known to decompose by the following routes.

$$Cu(OH)_2 \rightarrow CuO + H_2O \quad (R1)$$

$$Cu(NO_3)_2 \rightarrow CuO + 2\,NO_2^{\bullet} + 1/2\,O_2 \quad (R2)$$

Fig. 2 demonstrates the formation of H_2O, O_2 and $NO_2^{\bullet}$, as would be expected from these decomposition routes. Adding both sides of R1 and R2, the primary pyrolysis route for BCN can be written as follows.

$$Cu_2(NO_3)(OH)_3 \rightarrow 2\,CuO + 3/2\,H_2O + NO_2^{\bullet} + 1/4\,O_2 \quad (R3)$$

Followed the initial decomposition, small portions of the $NO_2^{\bullet}$ produced from the $Cu(NO_3)_2$ and the H_2O generated from the $Cu(OH)_2$ react to form HNO_3 according to:

$$2\,NO_2^{\bullet} + H_2O \rightarrow HNO_3 + HONO \quad (R4)$$

This reaction generates the HNO_3 that is evident in Fig. 2. The other product HONO is thermally unstable and undergoes the following autoredox reaction at high temperature, which also generates a small amount of $NO^{\bullet}$.

$$3\,HONO \rightarrow HNO_3 + 2\,NO^{\bullet} + H_2O \quad (R5)$$

3.2. TG/DSC/HRMS analysis of gas evolution with GN

Fig. 3 shows the TG/DSC/HRMS results obtained from heating the GN. The TG/DSC data (Fig. 3(a)) demonstrate two endothermic peaks; one at 213 °C without a mass change that is associated with melting, and the other with a mass loss between approximately 260 and 335 °C due to pyrolysis. This thermal behavior is fairly typical and similar results have been reported in the literature [9,10]. Approximately 25 % of the original mass remained after heating to 350 °C as a solid residue, and GN is known to produce a solid that consists of polymers such as melamine and melon derived from the intermediate compound HNCNH [8,13].

The HRMS data exhibit peaks at m/z values of 17.0073 (OH^+), 17.0305 (NH_3^+), 18.0153 (H_2O^+), 28.0101 (CO^+), 28.0134 (N_2^+), 30.0061 (NO^+), 43.0247 ($HNCO^+$), 44.0095 (CO_2^+), 44.0128 (N_2O^+) and 46.0055 (NO_2^+), and the variations in the peak intensities with temperature are shown in Fig. 3(b). The primary evolved gases were determined to be NH_3, H_2O, CO, N_2, $NO^{\bullet}$, HNCO, CO_2, N_2O and $NO_2^{\bullet}$. Although these products have all been qualitatively identified in prior studies [8–11], the present HRMS data clearly distinguished between 17.0073 (OH^+) and 17.0305 (NH_3^+), and between 44.0095 (CO_2^+) and 44.0128 (N_2O^+).

The experimental HRMS profiles were corrected based on the fragmentation ratio method and the associated calculations are presented below as Eqs. 6 through 14. The fragmentation ratios are provided in a NIST database [19] while that for HNCO can be found in the literature [21].

$$I^{\text{total}}_{NO_2\cdot} \cong I^{46.0055}_{NO_2^+} + I^{30.0061}_{NO^+(NO_2^+)} = I^{46.0055}_{NO_2^+} + \frac{3703}{9999} I^{46.0055}_{NO_2^+} \quad (6)$$

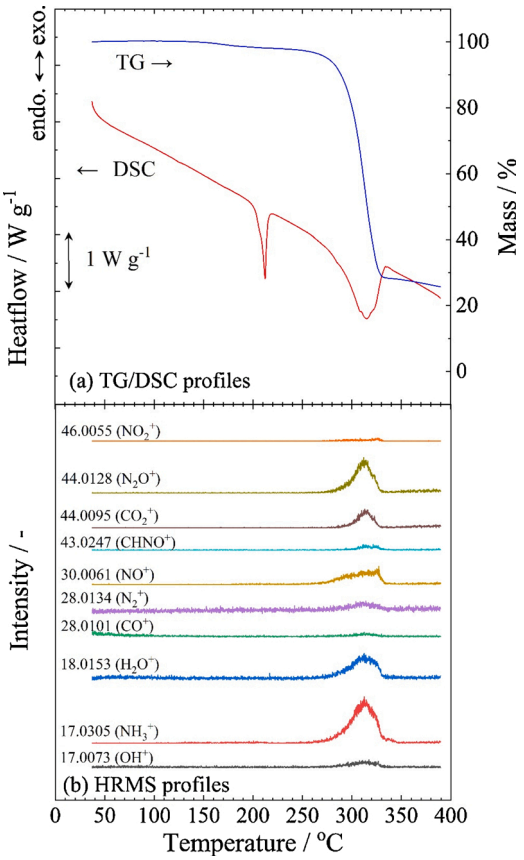

Fig. 3. (a) TG/DSC data and (b) HRMS profiles obtained from GN at a heating rate of 10 °C min^{-1}.

$$I_{N_2O}^{total} \cong I_{N_2O^+}^{44.0128} + I_{NO^+(N_2O^+)}^{30.0061} + I_{N_2^+(N_2O^+)}^{28.0134} = I_{N_2O^+}^{44.0128} + \frac{3113}{9999} I_{N_2O^+}^{44.0128} + \frac{1008}{9999} I_{N_2O^+}^{44.0128} \quad (7)$$

$$I_{CO_2}^{total} \cong I_{CO_2^+}^{44.0095} + I_{CO^+(CO_2^+)}^{28.0101} = I_{CO_2^+}^{44.0095} + \frac{981}{9999} I_{CO_2^+}^{44.0095} \quad (8)$$

$$I_{HNCO}^{total} \cong I_{HNCO^+}^{43.0247} + I_{CNO^+(HNCO^+)}^{42.0168} + I_{HCO^+(HNCO^+)}^{29.0180} = I_{HNCO^+}^{43.0247} + \frac{21.7}{100} I_{HNCO^+}^{43.0247} + \frac{13.8}{100} I_{HNCO^+}^{43.0247} \quad (9)$$

$$I_{NO\cdot}^{total} \cong I_{NO^+}^{30.0061} - I_{NO^+(N_2O^+)}^{30.0061} - I_{NO^+(NO_2^+)}^{30.0061} = I_{NO^+}^{30.0061} - \frac{3113}{9999} I_{N_2O^+}^{44.0128} - \frac{9999}{3703} I_{NO_2^+}^{46.0055} \quad (10)$$

$$I_{N_2}^{total} \cong I_{N_2^+}^{28.0134} - I_{N_2^+(N_2O^+)}^{28.0134} + \frac{1}{2} I_{N^+}^{14.0067} = I_{N_2^+}^{28.0134} - \frac{1008}{9999} I_{N_2O^+}^{44.0128} + \frac{1}{2} \frac{1379}{9999} \left(I_{N_2^+}^{28.0134} - \frac{1008}{9999} I_{N_2O^+}^{44.0128} \right) \quad (11)$$

$$I_{CO}^{total} \cong I_{CO^+}^{28.0101} - I_{CO^+(CO_2^+)}^{28.0101} = I_{CO^+}^{28.0101} - \frac{981}{9999} I_{CO_2^+}^{44.0095} \quad (12)$$

$$I_{H_2O}^{total} \cong I_{H_2O^+}^{18.0153} + I_{OH^+(H_2O^+)}^{17.0073} = I_{H_2O^+}^{18.0153} + \frac{2122}{9999} I_{H_2O^+}^{18.0153} \quad (13)$$

$$I_{NH_3}^{total} \cong I_{NH_3^+}^{17.0305} + I_{NH_2^+(NH_3^+)}^{16.0226} = I_{NH_3^+}^{17.0305} + \frac{8007}{9999} I_{NH_3^+}^{17.0305} \quad (14)$$

Fig. 4 plots the evolution of various gaseous products from GN at a heating rate of 10 °C min^{-1} and establishes that NH_3, H_2O, N_2, HNCO, CO_2, N_2O, and $NO_2^{\cdot}$ were all obtained. NH_3 first appeared at 260 °C, at which point an endothermic reaction also began, while the evolution of

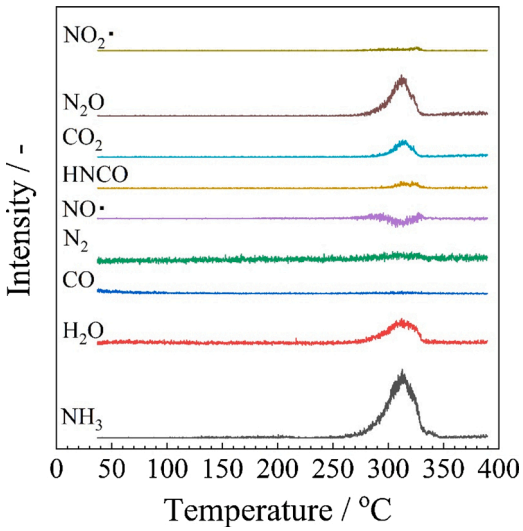

Fig. 4. The gas evolution behavior of GN at 10 °C min^{-1} based on MS data.

the other gases followed at approximately 280 °C. The peaks at *m/z* values of 28.0101 (CO^+) and 30.0061 (NO^+) were reduced by the fragmentation corrections, showing that only very small amounts of CO and $NO^{\cdot}$ were actually generated.

The mechanism proposed in our previous theoretical study [22] can be used to explain the gas evolution behavior observed in this work. Our prior research investigated various sets of GN reactions using quantum chemistry calculations and identified the most probable reaction scheme on a thermodynamic basis. However, these theoretical predictions required experimental validation. Although experimental data exist to support our proposed reaction process, the TG/DSC/HRMS results presented herein provide more definitive validation.

Based on this mechanism, the initial pyrolysis proceeds endothermically via two different paths involving either decomposition of CN_3H_5 or reaction between CN_3H_5 and HNO_3. Both paths equate to the same overall reaction:

$$GN \rightarrow CH_5N_3 + HNO_3 \rightarrow HNCNH + NH_3 + HNO_3 \quad (R6)$$

The NH_3 from this initial pyrolysis is that identified in the HRMS profiles in Fig. 4. HNCNH (*m/z* 42) was not found in the evolved gases, and so evidently remained in the liquid phase or was consumed in some manner. HNCNH is known to undergo exothermic polymerization to produce materials such as melamine and melon, which would form a solid residue. Another possibility is that this compound is oxidized by HNO_3, starting with homolysis of the HO-NO_2 bond, as in the reaction below. The energy barrier to this bond cleavage is high, and so it is likely that the cleavage occurs above approximately 280 °C [23–25]. The temperature at which the pyrolysis was observed to occur was therefore sufficient to homolytically decompose HNO_3.

$$HNO_3 \rightarrow OH^{\cdot} + NO_2^{\cdot} \quad (R7)$$

The formation of $NO_2^{\cdot}$ but not $OH^{\cdot}$ is evident above 280 °C in Fig. 4. However, $OH^{\cdot}$ is a highly reactive radical, and so would be expected to rapidly react with other compounds. The $OH^{\cdot}$ and $NO_2^{\cdot}$ radicals resulting from the above reaction could attack HNCNH to form N_2O and HNCO, the latter of which then decomposes to CO_2 as shown below [22,23].

$$HNCNH + OH^{\cdot} \rightarrow HNCN^{\cdot} + H_2O \quad (R8)$$

$$HNCN^{\cdot} + NO_2^{\cdot} \rightarrow HNCO + N_2O \quad (R9)$$

The HNCO generated in this process reacts with H_2O to form NH_3 and CO_2 based on the following reaction, both of which are found in Fig. 4.

$$HNCO + H_2O \rightarrow NH_3 + CO_2 \quad (R10)$$

The generation of a small amount of N_2 can be seen in Fig. 4, and this is thought to have resulted from a free radical reaction between NH_3 and HNO_3. NH_3 is thermally stable and difficult to oxidize, but a small amount of this compound was evidently attacked by radicals to produce N_2 and H_2O [26,27].

3.3. TG/DSC/HRMS analysis of gas evolution from GN/BCN

Fig. 5 presents the TG/DSC/HRMS results for GN/BCN mixtures. Comparing these results to the data obtained from pure BCN and GN, it is apparent that the thermal behavior of GN/BCN mixtures differed drastically from that of the components. Here, the thermal behavior (shown in Fig. 5(a)) can be divided into two regions from 133 to 210 °C (termed pyrolysis I) and 210–275 °C (pyrolysis II). Pyrolysis I begins with an endothermic reaction associated with a mass loss at approximately at 133 °C, followed by an exothermic reaction at 169 °C. The following pyrolysis II starts at 210 °C with a sharp endothermic peak that corresponds to the melting point of GN (213 °C). Immediately following melting, an exothermic reaction with rapid heat flow and mass loss occurs.

Fig. 5(b) demonstrates the variations in gas evolution with increasing temperature based on the HRMS profiles. Peaks are present at *m/z* values of 17.0073 (OH^+), 17.0305 (NH_3^+), 18.0153 (H_2O^+), 28.0101 (CO^+), 28.0134 (N_2^+), 30.0061 (NO^+), 44.0095 (CO_2^+), and 44.0128 (N_2O^+). These peaks were also corrected based on fragmentation ratios, using Eqs. 6 through 14.

Fig. 6 summarizes the variations in mass, heat flow and gas evolution with temperature. Comparing these data to those acquired from pure BCN (Fig. 2) and GN (Fig. 4), the generation of gaseous products from a GN/BCN mixture is seen to be significantly different. Specifically, the mixture produced less HNO_3 and $NO_2^{\bullet}$ compared to pure BCN and less

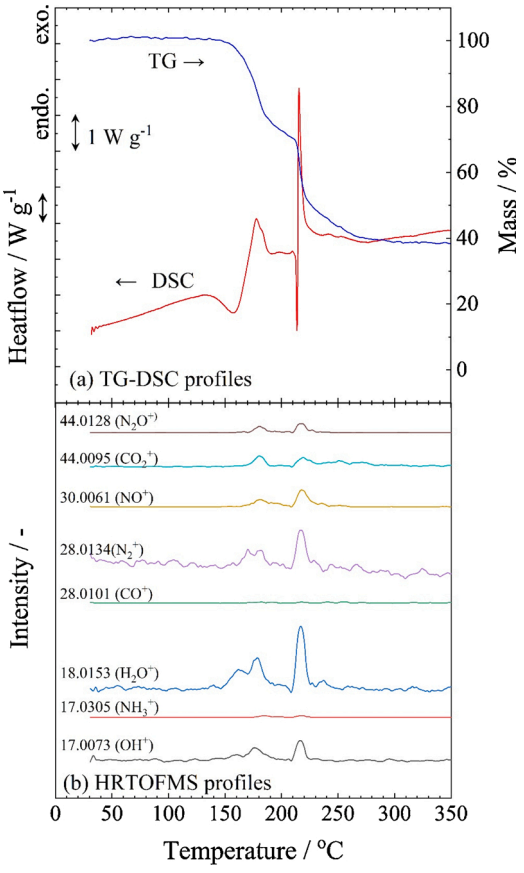

Fig. 5. (a) TG-DSC data and (b) HRMS profiles obtained from a GN/BCN mixture at a heating rate of 5 °C min^{-1}.

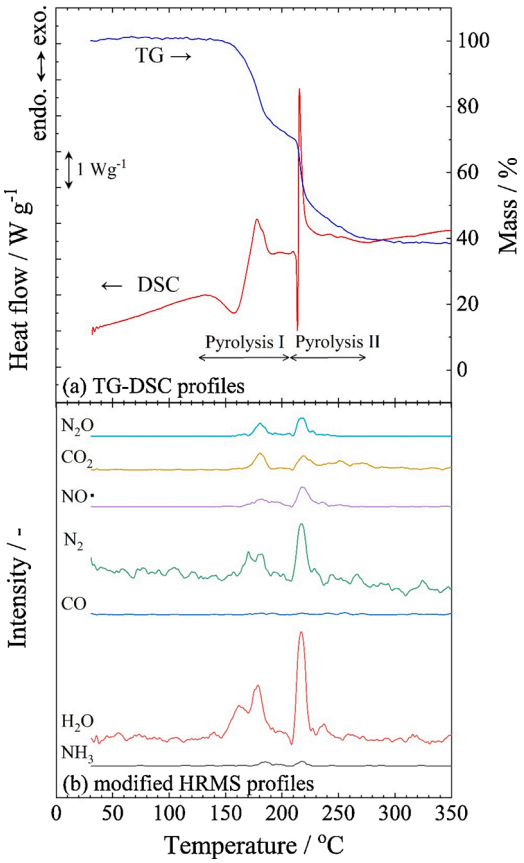

Fig. 6. (a) TG-DSC data and (b) the gas evolution behavior obtained from a GN/BCN mixture at 5 °C min^{-1}.

NH_3 and HNCO but more H_2O, N_2, and CO_2 compared to pure GN.

During the pyrolysis I phase, gas evolution began with the endothermic formation of H_2O at 130 °C, after which N_2, $NO^{\bullet}$, CO_2, N_2O and additional H_2O were generated at 160 °C in an exothermic process. In this temperature range, both GN and BCN are solids, and so the pyrolysis reactions likely took place at points of contact between the powder surfaces. In one possible reaction, GN dissociates to give HNO_3 and CN_3H_5, as follows.

$$GN \rightarrow HNO_3 + CH_5N_3 \quad \text{(R11)}$$

The strong acid HNO_3 would neutralize the weak base copper(II) hydroxide to produce copper(II) nitrate and free H_2O as in the reaction below.

$$Cu(OH)_2 + 2HNO_3 \rightleftarrows Cu(NO_3)_2 + 2H_2O \quad \text{(R12)}$$

This would explain the H_2O detected beginning at 130 °C. The guanidine moiety in the GN would undergo pyrolysis to form HNCNH and NH_3 as showed in the section 3.2. To explain pyrolysis mechanisms of a composition involving NH_3, HNO_3, and copper(II) nitrate, the mechanism established for ammonium nitrate (the salt of NH_3 and HNO_3) and copper(II) nitrate/oxide mixtures [28–30] can be used. Tetra- or di-ammine copper(II) complexes were produced from a mixture of Cu $(NO_3)_2$ and ammonium nitrate upon heating in the range of 160–220 °C [30]. In temperature range of pyrolysis of GN/BCN mixture, the di-ammine complex ($[Cu(NH_3)_2](NO_3)_2$) would preferentially form. NH_3 from GN would react with copper(II) nitrate to form copper ammine complexes as in the reaction below.

$$Cu(NO_3)_2 + 2NH_3 \rightleftarrows [Cu(NH_3)_2](NO_3)_2 \quad \text{(R13)}$$

The $[Cu(NH_3)_2](NO_3)_2$ can be hydrolyzed to basic copper(II) nitrate,

NH_3, and HNO_3 [31]. Although reactions R12 and R13 are reversible, elimination of H_2O to gas-phase enhances forward reactions. Copper(II) ammine complex is a highly reactive material and it is known to have explosion properties equal to initiation explosives (low impact-sensitivity, large heat of combustion, and high burning rate) [32, 33]. Production of $[Cu(NH_3)_2](NO_3)_2$ would play an important role in pyrolysis of GN/BCN mixture. This ammine complex promptly pyrolyze to produce CuO, N_2 H_2O, and $NO_2^{\bullet}$ with large exothermic heats [30].

$$2[Cu(NH_3)_2](NO_3)_2 \rightarrow 2\ CuO + 3\ N_2 + 6\ H_2O + 2\ NO_2^{\bullet} \quad (R14)$$

This chemical reaction can explain evolving large amounts of N_2 and H_2O and few of NH_3 from GN/BCN (Fig. 6). The CuO and HNO_3 would also be expected to react to regenerate $Cu(NO_3)_2$, as follows.

$$CuO + 2HNO_3 \rightarrow Cu(NO_3)_2 + H_2O \quad (R15)$$

The $Cu(NO_3)_2$ would react with NH_3 to form $[Cu(NH_3)_2](NO_3)_2$ again (R13). This cycle would therefore catalytically decompose (persistent and toxic) NH_3 to N_2 and H_2O, and the $NO_2^{\bullet}$ from R14 would be consumed to produce $NO^{\bullet}$ according to reactions R4 and R5.

The gases generated during the pyrolysis II stage and their corresponding peak intensities were similar to those produced in the pyrolysis I region, and so the reaction scheme was also likely similar to that shown above. The pyrolysis II process starts with melting of the GN, after which the molten GN surrounds the solid BCN such that the contact area is greatly increased compared to the solid-solid reaction process in the pyrolysis I phase. In addition, the temperature at which the pyrolysis II stage begins equals the pyrolysis point of BCN, and this is expected to enhance the pyrolysis of the GN/BCN mixture. Thus, the reaction rate is increased and more heat is released.

During the pyrolysis of the GN/BCN mixture, the chemical and physical properties of the components and the intermediate species combined to enhance each reaction. Fig. S1 in the Supporting Information provides a summary of the thermal characteristics obtained from TA-EGA and the proposed chemical reaction equations for the pure GN and BCN and for the GN/BCN mixture. As noted, the pyrolysis II stage of the GN/BCN includes the melting points of GN and the pyrolysis temperature of BCN. In addition, the initial intermediate species NH_3 and HNO_3 produced by the GN can be catalytically decomposed on copper (II) nitrate and copper(II) oxide generated by the BCN. We therefore believe that the improved performance of the mixture of the two compounds is derived from these synergistic effects.

4. Conclusion

This work performed a detailed investigation of the thermal properties and gas evolution characteristics of GN/BCN mixtures, which are used as gas generators in automobile airbag systems. HRMS was employed to distinguish between different species having similar masses, such as CO_2 and N_2O, based on rapid scanning and acquisition of the full mass spectra of the fragment ions of compounds on an accurate mass basis. The HRMS data were also modified by correcting the apparent intensities of the fragments by summing related peaks and subtracting overlapping unrelated peaks, to obtain the true intensities of the various gases. This correction prevented overestimation of the amounts of certain evolved gases. This research demonstrates that TG/DSC/HRMS is a powerful tool for assessing the pyrolysis of energetic materials, and is superior to standard MS and IR-based approaches especially when combined with thermal analysis.

Possible schemes for the pyrolysis of pure GN and BCN and of a GN/BCN mixture were determined based on TA-EGA data. The pyrolysis of BCN was proposed to proceed based on the simultaneous reactions of copper(II) nitrate and copper(II) hydroxide, with H_2O, O_2, $NO_2^{\bullet}$ and HNO_3 as the main gaseous products. GN was determined to undergo pyrolysis via the reaction series GN → $CH_5N_3 + HNO_3$ → HNCNH + NH_3 + HNO_3. The HNCNH is subsequently attacked by $OH^{\bullet}$ and $NO_2^{\bullet}$ radicals generated by the homolysis of HNO_3 to form N_2O and HNCO. In the case of GN/BCN pyrolysis, the mechanisms described above for pure GN and BCN work in concert and enhance one another. As a result, the toxic NH_3 normally produced by the pyrolysis of GN is effectively decomposed into N_2 and H_2O. This intermeshing of various reaction mechanisms explains why the GN/BCN combination provides exceptional performance as a gas generating agent.

CRediT authorship contribution statement

Yu-ichiro Izato: Conceptualization, Writing - original draft, Methodology. **Kento Shiota:** Writing - review & editing, Resources, Formal analysis, Visualization. **Kenta Satoh:** Methodology, Data curation. **Takashi Satoh:** Methodology, Data curation. **Yukinori Yahata:** Methodology, Data curation. **Atsumi Miyake:** Writing - review & editing, Supervision, Funding acquisition.

Declaration of Competing Interest

The authors report no declarations of interest.

Acknowledgement

This research was supported by the Foundation for the Promotion of Industrial Explosives Technology 2020 and the JSPS KAKENHI [grant numbers 20H00287 and 20K14993]

Appendix A. Supplementary data

Supplementary material related to this article can be found, in the online version, at doi:https://doi.org/10.1016/j.jaap.2020.104918.

References

[1] Y.D. Seo, S.H. Chung, J.J. Yoh, Automotive airbag inflator analysis using the measured properties of modern propellants, Fuel 90 (2011) 1395–1401, https://doi.org/10.1016/j.fuel.2010.12.042.
[2] L. Ding, F.-Q. Zhao, Q. Pan, H.-X. Xu, Research on the thermal decomposition behavior of NEPE propellant containing CL-20, J. Anal. Appl. Pryolysis 121 (2016) 121–127, https://doi.org/10.1016/j.jaap.2016.07.012.
[3] M. Abd-Elghany, A. Elbeih, T.M. Klapötke, Thermo-analytical study of 2,2,2-trinitroethyl-formate as a new oxidizer and its propellant based on a GAP matrix in comparison with ammonium dinitramide, J. Anal. Appl. Pryolysis 133 (2018) 30–38, https://doi.org/10.1016/j.jaap.2018.05.004.
[4] M. Abd-Elghany, T.M. Klapötke, A. Elbeih, Investigation of 2,2,2-trinitroethyl-nitrocarbamate as a high energy dense oxidizer and its mixture with Nitrocellulose (thermal behavior and decomposition kinetics), J. Anal. Appl. Pryolysis 128 (2017) 397–404, https://doi.org/10.1016/j.jaap.2017.09.010.
[5] A.-A.M. Gabera, C. Wentrup, Pyrolysis of hydrazine derivatives and related compounds with NN single bonds, J. Anal. Appl. Pryolysis 125 (2017) 258–278, https://doi.org/10.1016/j.jaap.2017.03.016.
[6] P. Ashutosh, A.A. Vargeese, Experimental and computational investigation on the decomposition kinetics and uni-molecular degradation of (Z)-N,2,2,2-tetranitroacetimidic acid, J. Anal. Appl. Pryolysis 135 (2018) 281–288, https://doi.org/10.1016/j.jaap.2018.08.025.
[7] J. Zhou, L. Ding, F. Bi, B. Wang, J. Zhang, Research on the thermal behavior of novel heat resistance explosive 5,5′-bis(2,4,6-trinitrophenyl)-2,2′-bi(1,3,4-oxadiazole), J. Anal. Appl. Pryolysis 129 (2018) 189–194, https://doi.org/10.1016/j.jaap.2017.11.013.
[8] A. Sankaranarayanan, L. Mallick, N.R. Kumbhakarna, A numerical and experimental study of the decomposition pathways of guanidinium nitrate, J. Therm. Anal. Calorim. 131 (2018) 427–441, https://doi.org/10.1007/s10973-017-6707-4.
[9] M. Nakashima, T. Itaura, H. Matsunaga, E. Higashi, S. Takagi, K. Katoh, A fundamental study on the thermal decomposition and combustion behaviors of guanidine nitrate and basic copper nitrate mixture, J. Therm. Anal. Calorim. 131 (2018) 95–100, https://doi.org/10.1007/s10973-017-6718-1.
[10] X. Mei, Y. Cheng, Y. Li, X. Zhu, S. Yan, X. Li, Thermal decomposition properties of guanidine nitrate and basic cupric nitrate, J. Therm. Anal. Calorim. 114 (2013) 131–135, https://doi.org/10.1007/s10973-012-2851-z.
[11] S. Yoshino, A. Miyake, Thermal decomposition properties of 1,2,4-triazole-3-one and guanidine nitrate mixtures, J. Therm. Anal. Calorim. 102 (2010) 513–516, https://doi.org/10.1007/s10973-010-0976-5.
[12] Y. Liu, X. Wang, C.-m. Shu, Y. Wang, D. Zhao, W. Chen, J. Zhang, J. Yin, Thermal hazard evolution on guanidine nitrate, J. Therm. Anal. Calorim. 131 (2018) 95–100, https://doi.org/10.1007/s10973-018-7148-4.

[13] M.R. Udupa, Thermal decomposition of guanidine nitrate, Thermochim. Acta 53 (1982) 383–385, https://doi.org/10.1016/0040-6031(82)85034-X.
[14] A. Benhammada, D. Trache, Thermal decomposition of energetic materials using TG-FTIR and TG-MS: a state-of-the-art review, Appl. Spectrosc. Rev. (2020), https://doi.org/10.1080/05704928.2019.1679825.
[15] M. Kaniewski, K. Hoffmann, J. Hoffmann, Influence of selected potassium salts on thermal stability of ammonium nitrate, Thermchim. Acta 678 (2019) 178313, https://doi.org/10.1016/j.tca.2019.178313.
[16] U. Swami, K. Senapathi, K.M. Srinivasulu, J. Desingu, A. Chowdhury, Energetic ionic liquid hydroxyethylhydrazinium nitrate as an alternative monopropellant, Combust. Flame 215 (2020) 93–102, https://doi.org/10.1016/j.combustflame.2020.01.025.
[17] H. Matsunaga, K. Katoh, H. Habu, M. Noda, A. Miyake, Thermal behavior of ammonium dinitramide and amine nitrate mixtures, J. Therm. Anal. Calorim. 135 (2019) 2677–2685, https://doi.org/10.1007/s10973-018-7875-6.
[18] G. Santhosh, P.B. Soumyamol, M. Sreejith, S. Reshmi, Isoconversional approach for the non-isothermal decompositionkinetics of guanylurea dinitramide (GUDN), Thermochim. Acta 632 (2016) 46–51, https://doi.org/10.1016/j.tca.2016.03.019.
[19] P.J. Linstrom, W.G. Mallard, in: NIST Standard Reference Database Number 69 (Ed.), NIST Chemistry WebBook, National Institute of Standards and Technology, 2020. Accessed 30 May 24 2020, http://webbook.nist.gov.
[20] R.A. Friedel, J.L. Shultz, A.G. Sharkey, Mass spectrum of nitric acid, Anal. Chem. 45 (1967) 1128, https://doi.org/10.1021/ac60150a615.
[21] D.J. Bogan, C.W. Hand, Mass spectrum of isocyanic acid, J. Phys. Chem. 75 (1971) 1532–1536, https://doi.org/10.1021/j100680a026.
[22] Y. Izato, A. Miyake, Initial decomposition pathways of guanidium nitrate studied by quantum chemistry calculation, Sci. Technol. Energ. Matter. 79 (2018) 80–88.
[23] Y. Izato, A. Miyake, A detailed chemical kinetics model for the combustion of gas-phase guanidine nitrate, Sci. Technol. Energ. Matter. 79 (2018) 166–174.
[24] K.R. Brower, J.C. Oxley, M.P. Tewari, Evidence for homolytic decomposition of ammonium nitrate at high temperature, J. Phys. Chem. 93 (1989) 4029–4033, https://doi.org/10.1021/j100347a033.
[25] J. Park, M.C. Lin, Thermal decomposition of gaseous ammonium nitrate at low pressure: kinetic modeling of product formation and heterogeneous decomposition of nitric acid, J. Phys. Chem. A 113 (2009) 13556–13561, https://doi.org/10.1021/jp9058005.
[26] Y. Izato, A. Miyake, Kinetic analysis of the thermal decomposition of liquid ammonium nitrate based on thermal analysis and detailed reaction simulations, J. Therm. Anal. Calorim. 134 (2018) 813–823, https://doi.org/10.1007/s10973-018-7322-8.
[27] Y. Izato, A. Miyake, A detailed chemical kinetic model for the combustion of gas phase ammonium nitrate, Sci. Technol. Energ. Mater. 78 (2018) 143–149.
[28] Y. Izato, K. Kajiyama, A. Miyake, Thermal decomposition mechanism of ammonium nitrate and copper (II) oxide mixtures, Sci. Technol. Energ. Mater. 75 (2014) 128–133.
[29] H. Matsunaga, Y. Izato, H. Habu, A. Miyake, Thermal decomposition characteristics of mixtures of ammonium dinitramide and copper (II) oxide, J. Therm. Anal. Calorim. 121 (2015) 319–326, https://doi.org/10.1007/s10973-015-4645-6.
[30] I.V. Morozov, A.A. Fedorova, A.V. Knotko, O.R. Valedinskaja, E. Kemnitz, Mixed 3d-metal oxides prepared using molten ammonium nitrate, Mendeleev Commun. 14 (2004) 138–139, https://doi.org/10.1070/MC2004v014n04ABEH001951.
[31] S.S. Dyukarey, I.V. Morozov, L.N. Reshetova, O.V. Guz', I.V. Arkhangel'skii, Y. M. Korenev, F.M. Spiridonov, Copper(II) nitrate ammoniates $Cu(NH_3)_4(NO_3)_2$ and $Cu(NH_3)_2(NO_3)_2$ and their thermolysis under reduced pressure, Russ. J. Inorg. Chem. 44 (1999) 3–8.
[32] W.R. Tomlinson, K.G. Ottoson, L.F. Audrieth, Explosive properties of metal ammines, J. Am. Chem. Soc. 71 (1949) 375–376, https://doi.org/10.1021/ja01169a519.
[33] V.V. Gorbunov, L.F. Shmagin, Burning of copper (II) tetramine salts, Combust. Explos. Shock Waves 8 (1972) 429–431, https://doi.org/10.1007/BF00741198.